

Article

# Sucrose-Assisted Synthesis of Layered Lithium-Rich Oxide $\text{Li}[\text{Li}_{0.2}\text{Mn}_{0.56}\text{Ni}_{0.16}\text{Co}_{0.08}]\text{O}_2$ as a Cathode of Lithium-Ion Battery

Xueyin Song<sup>1</sup>, Haifu Huang<sup>2,\*</sup> and Wei Zhong<sup>1,\*</sup>

<sup>1</sup> Collaborative Innovation Center of Advanced Microstructures, National Laboratory of Solid State Microstructures and Jiangsu Provincial Laboratory for Nanotechnology, Nanjing University, Nanjing 210093, China

<sup>2</sup> Guangxi Key Laboratory for Relativistic Astrophysics, Center on Nanoenergy Research, Guangxi Novel Battery Materials Research Center of Engineering Technology, Guangxi Colleges and Universities Key Laboratory of Novel Energy Materials and Related Technology, Guangxi Key Laboratory of Processing for Non-ferrous Metallic and Featured Materials, School of Physics Science and Technology, Guangxi University, Nanning 530004, China

\* Correspondence: huanghf@gxu.edu.cn (H.H.); wzhong@nju.edu.cn (W.Z.)

Received: 27 June 2019; Accepted: 18 August 2019; Published: 21 August 2019



**Abstract:** Herein, the lithium-rich material  $\text{Li}[\text{Li}_{0.2}\text{Mn}_{0.56}\text{Ni}_{0.16}\text{Co}_{0.08}]\text{O}_2$  is successfully prepared by a sucrose-assisted gel method. With the assistance of sucrose,  $\text{Li}[\text{Li}_{0.2}\text{Mn}_{0.56}\text{Ni}_{0.16}\text{Co}_{0.08}]\text{O}_2$  precursors can be uniformly dispersed into sticky sucrose gel without aggregation. XRD shows that the lithium-rich material  $\text{Li}[\text{Li}_{0.2}\text{Mn}_{0.56}\text{Ni}_{0.16}\text{Co}_{0.08}]\text{O}_2$  has a well-organized layered structure. The electrochemical performance is influenced by calcination temperature. The results show that the sample  $\text{Li}[\text{Li}_{0.2}\text{Mn}_{0.56}\text{Ni}_{0.16}\text{Co}_{0.08}]\text{O}_2$  calcined at 900 °C possess significant performance. This sample delivers higher discharge specific capacity of 252 mAh g<sup>-1</sup>; rate capability with a capacity retention of 86% when tested at 5C; and excellent cyclic stability with a capacity retention rate of 81% after 100 cycles under 1C test. The sucrose-assisted method shows great potential in fabricating layered lithium-rich materials.

**Keywords:** layered lithium-rich materials; cathode material; sucrose-assisted method; electrochemical performance

## 1. Introduction

Lithium-ion batteries (LIBs) are widely used in consumer electronics, electric vehicle (EVs), and hybrid electric vehicles (HEVs), due to their high specific capacity, long cycle life and environmental friendliness [1–4]. However, the energy density of LIBs still needs to increase to meet current needs. Among a variety of factors associated with performance, the electrode material is a major factor in determining the electrochemical performance [5]. Currently, cathode materials, including  $\text{LiCoO}_2$  (LCO, ~140 mAh g<sup>-1</sup>) [6],  $\text{LiFePO}_4$  (LFP, ~170 mAh g<sup>-1</sup>) [7], and  $\text{LiMn}_2\text{O}_4$  (spinel, ~120 mAh g<sup>-1</sup>) [8], show relatively lower specific capacity (<200 mAh g<sup>-1</sup>) than that of anode material, such as graphite and Si-based composites (>300 mAh g<sup>-1</sup>) [9,10], which hinder development of LIBs with high energy density. In other words, improvement of the specific capacity and energy density is largely dependent on the development of innovative cathode materials [11–13]. Therefore, there is an urgent need to develop high-performance cathode materials. Thereby, cathode materials with high capacity and high rate have been attracted great attention.

Among these innovative materials, layered lithium-rich ones are extraordinarily attractive for the cathode electrode of a battery, due to high discharge capacity of over 250 mAh g<sup>-1</sup>, high

operating potentials (4.8–2.0 V), and a well-organized layered structure [14,15]. In general, lithium-rich materials contain two types of phase structure: the  $\text{Li}_2\text{MnO}_3$  phase and  $\text{LiMO}_2$  phase ( $M = \text{Ni, Co, Mn}$ ) [16]. Therefore, lithium-rich cathode materials can be marked as  $x\text{Li}_2\text{MnO}_3 \cdot (1-x)\text{LiMO}_2$  ( $M = \text{Ni, Co, Mn, } 0 \leq x \leq 1$ ), the stability of the corresponding structures is better than the pure  $\text{Li}_2\text{MnO}_3$ . Moreover, as compared to commercial  $\text{LiCoO}_2$ , lithium-rich cathode materials are safer, environment-friendly, and lower cost, due to a large amount of Mn. It is worth noting that the Co element in layered lithium-rich materials plays an important role in reducing the electrode polarization and improving  $\text{Li}_2\text{MnO}_3$  activation. Therefore, the lithium-rich materials  $\text{Li}[\text{Li}_{0.2}\text{Mn}_{0.54}\text{Ni}_{0.13}\text{Co}_{0.13}]\text{O}_2$  (marked as  $0.6\text{Li}_2\text{MnO}_3 \cdot 0.4\text{LiMn}_{1/3}\text{Ni}_{1/3}\text{Co}_{1/3}\text{O}_2$ ) exhibit better lithium storage performance than  $\text{Li}[\text{Li}_{0.2}\text{Mn}_{0.6}\text{Ni}_{0.2}]\text{O}_2$  (marked as  $0.6\text{Li}_2\text{MnO}_3 \cdot 0.4\text{LiMn}_{0.5}\text{Ni}_{0.5}\text{O}_2$ ).

However, there exist some disadvantages for further commercial application of layered lithium-rich materials, such as its larger irreversible capacity losses, poor cyclic stability, and low rate capability [17]. So far, significant efforts have been focused on the improvement of the electrochemical performance of these layered lithium-rich cathodes. The main strategy is to add a protective layer, such as  $\text{Al}_2\text{O}_3$ ,  $\text{AlF}_3$ , and  $\text{LiF}$  on the surface of lithium-rich materials through surface modification. The rate capability and the cyclic stability have been improved greatly under the synergy of a protective layer and layered lithium-rich cathodes [18–20]. However, these coating materials also increase the interfacial resistance, decrease the specific capacity and energy density, due to their insulativity. In addition, the coating process of the protective layer is quite complicated, which will increase the cost of production. With the development of nanotechnology, the introduction of the nanostructure can improve the rate capability and the cyclic stability of lithium-rich materials to some extent [21–23]. In addition, the co-precipitation method is often used to prepare lithium-rich materials, but it is not easy to obtain phase-pure composite and nanostructure materials. Therefore, many challenges still exist to achieve better performance for layered lithium-rich materials with a nanostructure.

In this work,  $\text{Li}[\text{Li}_{0.2}\text{Mn}_{0.56}\text{Ni}_{0.16}\text{Co}_{0.08}]\text{O}_2$  was prepared by a sucrose-assisted gel method followed by calcination treatment.  $\text{Li}[\text{Li}_{0.2}\text{Mn}_{0.56}\text{Ni}_{0.16}\text{Co}_{0.08}]\text{O}_2$  precursors dispersed uniformly without aggregation. In the assistance of sucrose, the agglomeration of  $\text{Li}[\text{Li}_{0.2}\text{Mn}_{0.56}\text{Ni}_{0.16}\text{Co}_{0.08}]\text{O}_2$  particles was solved. The effect of different calcination temperature on morphology, structure, electrochemical properties was investigated to explore the best preparation route.

## 2. Experimental

### 2.1. The Preparation of $\text{Li}[\text{Li}_{0.2}\text{Mn}_{0.56}\text{Ni}_{0.16}\text{Co}_{0.08}]\text{O}_2$

The precursor solution was prepared by dissolving manganese acetate ( $\text{Mn}(\text{CH}_3\text{COO})_2 \cdot 4\text{H}_2\text{O}$ , 14 mmol), nickel acetate ( $\text{Ni}(\text{CH}_3\text{COO})_2 \cdot 4\text{H}_2\text{O}$ , 4 mmol), cobalt acetate ( $\text{Co}(\text{CH}_3\text{COO})_2 \cdot 4\text{H}_2\text{O}$ , 2 mmol), and lithium nitrate ( $\text{LiNO}_3$ , 31 mmol) in deionized water (100 mL), and then adding sucrose (31 mmol), and stirring at room temperature for 50 min on a magnetic stirrer. Then the precursor solution was dried at 90 °C for 5 h to evaporate half of the water. Finally, the obtained viscous solution was dried at 150 °C for 48 h again. In this process, the viscous solution underwent a series of changes to form a sticky gel with the evaporation of water, and in a short time, then sticky gel began to swell, and its volume increased. The loose solid gel was obtained after 48 h.

The loose solid gel was calcined under air atmosphere at 500 °C for 5 h, then at 700 °C for 1 h, and finally calcined at different temperatures (800 °C, 900 °C, and 1000 °C, marked as LNCM-800, LNCM-900, and LNCM-1000, respectively) for 15 h.

### 2.2. Electrochemical Measurements

The electrochemical performances were evaluated using 2032-type coin cells (MTI Corporation, Shanghai, China). The as-prepared lithium-rich material  $\text{Li}[\text{Li}_{0.2}\text{Mn}_{0.56}\text{Ni}_{0.16}\text{Co}_{0.08}]\text{O}_2$ , carbon black, and polyvinylidene fluoride (PVDF) were mixed in N-methyl-2-pyrrolidone (NMP) based on weight ratio (80:10:10) to form cathode slurry. Then the obtained slurry was coated on aluminum foil and

dried in a vacuum oven at 120 °C for 8 h to obtain the cathode sheet. The mass loading of the active material was  $\sim 1.82 \text{ mg cm}^{-2}$ . Lithium foil was used as a counter and the reference electrode. The coin cells assembled in an argon-filled glove box were composed of a cathode disk with a diameter of 10 mm and lithium foil by separator and using  $\text{LiPF}_6$  in EC: DMC as the electrolyte. Charge–discharge measurements under different C rates were performed on an Arbin electrochemical workstation (Arbin Instruments, College Station, Texas 77845, USA) in the range of 2.0 to 4.8 V. The cyclic voltammograms (CV) tests were performed on an electrochemical workstation (Gamry Reference 3000, Gamry Instruments, Westminster, PA, USA) at a scan rate of  $0.1 \text{ mV s}^{-1}$  in range of 2.0 to 5.0 V. The electrochemical impedance spectroscopy (EIS) was also performed on Gamry electrochemical workstation in range of 100 kHz to 0.01 Hz.

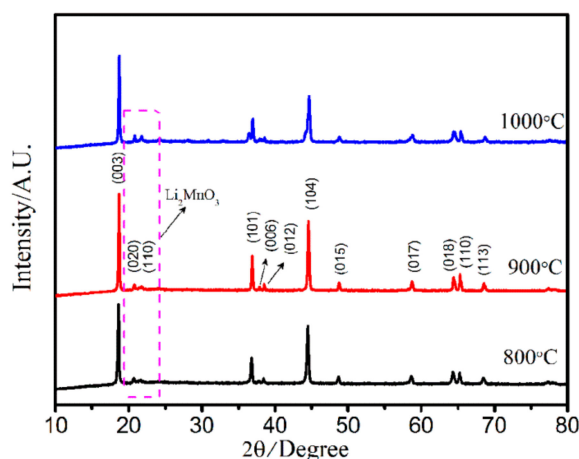
### 2.3. Material Characterizations

The structures and morphologies of the as-prepared  $\text{Li}[\text{Li}_{0.2}\text{Mn}_{0.56}\text{Ni}_{0.16}\text{Co}_{0.08}]\text{O}_2$  materials were recorded by using X-ray diffraction measurements (Rigaku Mini flex 600 diffractometer, Tokyo, Japan) and scanning electron microscopy (SEM, JSM-6510A, Tokyo, Japan), respectively.

## 3. Results and Discussion

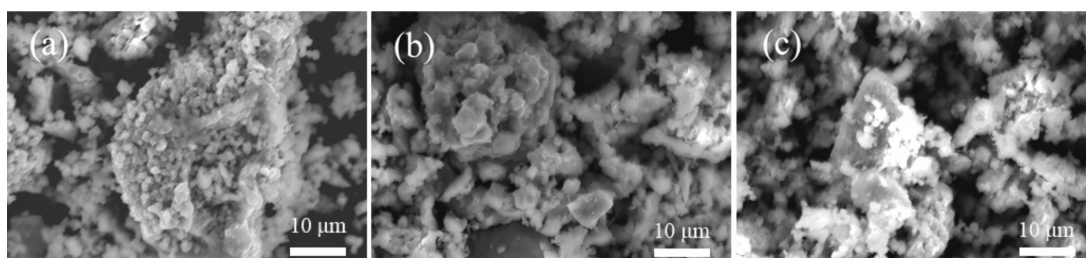
### 3.1. Analysis of Structure and Morphology

Figure 1 shows the XRD pattern of the  $\text{Li}[\text{Li}_{0.2}\text{Mn}_{0.56}\text{Ni}_{0.16}\text{Co}_{0.08}]\text{O}_2$  cathode material. All samples show a hexagonal  $\alpha\text{-NaFeO}_2$  layered structure with R-3m symmetry (PDF#70-2685) [24,25]. Two small satellite peaks located at near  $23^\circ$  indicate the presence of  $\text{Li}_2\text{MnO}_3$  with a C2/m space group [26]. For the samples LNCM-800 and LNCM-900, the clear splitting peaks (006)/(102) and (108)/(110) were observed in the XRD pattern, indicating a well-organized layered structure [27,28]. However, the peak intensity of LNCM-800 and LNCM-1000 was less than that of LNCM-900. Moreover, the splitting peaks in LNCM-1000 were hard to distinguish, suggesting a bad layered structure.



**Figure 1.** XRD patterns of  $\text{Li}[\text{Li}_{0.2}\text{Mn}_{0.56}\text{Ni}_{0.16}\text{Co}_{0.08}]\text{O}_2$  prepared at different temperature.

The SEM images of the  $\text{Li}[\text{Li}_{0.2}\text{Mn}_{0.56}\text{Ni}_{0.16}\text{Co}_{0.08}]\text{O}_2$  materials calcined at different temperatures were used to observe their morphology, as shown in Figure 2. It can be observed that the LNCM-800 exhibited a small grain with  $1 \mu\text{m}$  in size. When the temperature increased, the grain size of the LNCM-900 and LNCM-1000 became larger.



**Figure 2.** SEM images of  $\text{Li}[\text{Li}_{0.2}\text{Mn}_{0.56}\text{Ni}_{0.16}\text{Co}_{0.08}]\text{O}_2$  prepared at different temperature of (a) 800 °C, (b) 900 °C, (c) 1000 °C.

### 3.2. Electrochemical Properties

The electrochemical performance of  $\text{Li}[\text{Li}_{0.2}\text{Mn}_{0.56}\text{Ni}_{0.16}\text{Co}_{0.08}]\text{O}_2$  cathode material was evaluated by a charge–discharge test, electrochemical impedance spectroscopy (EIS) and cyclic voltammograms (CV). Figure 3a shows the initial charge–discharge curve of three samples. The initial charge curves display two platforms during the charging process: (i) A platform ranging from 3.9 to 4.5 V corresponded to the oxidation of metal ions ( $\text{Ni}^{2+}/\text{Ni}^{4+}$  and  $\text{Co}^{3+}/\text{Co}^{4+}$ ) and the extraction of  $\text{Li}^+$  from  $\text{LiMO}_2$  ( $M = \text{Ni}, \text{Co}, \text{Mn}$ ), (ii) another platform around 4.5 V is ascribed to the  $\text{Li}_2\text{MnO}_3$  activation process, which is a typical characteristic of layered lithium-rich material [29,30]. During this activation process,  $\text{Li}^+$  was extracted from the  $\text{Li}_2\text{MnO}_3$  phase accompanied by oxygen release and then formed the  $\text{Li}_2\text{O}$  component, resulting in an irreversible capacity loss [31,32]. But the process occurred only in the first charge process of lithium-rich material. Therefore, this is an irreversible structural phase transition. However, no platform could be observed during the discharge process, due to the merging of the voltage profiles. The first discharge capacity of LNCM-900 was higher, up to  $252 \text{ mAh g}^{-1}$  than that of LNCM-800 ( $219 \text{ mAh g}^{-1}$ ) and LNCM-1000 ( $171 \text{ mAh g}^{-1}$ ), suggesting that LNCM-900 should have the best electrochemical performance in all samples.

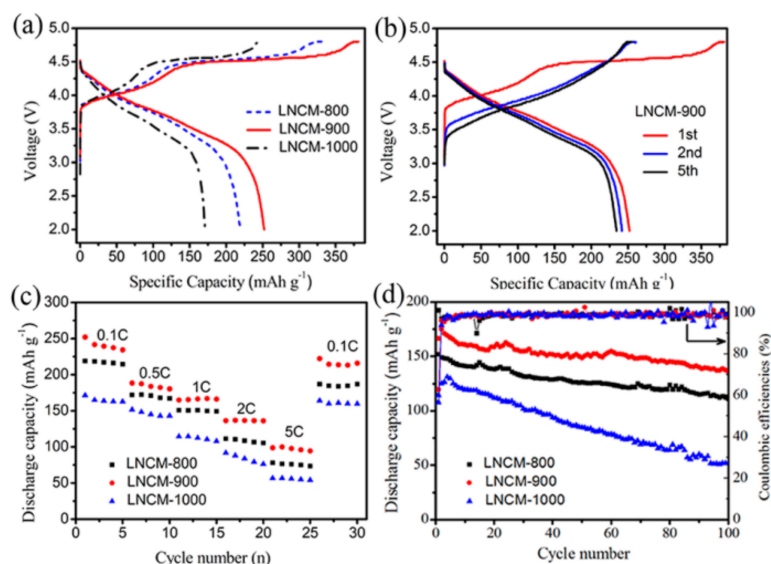


**Figure 3.** (a) Initial charge and discharge curves of LNCM-800, LNCM-900, and LNCM-1000 at 0.1C in the potential range from 2.0 to 4.8 V, (b) Charge–discharge curves of LNCM-900 at 0.1C, (c) The rate capability, (d) Cycle performance of all samples at 1 C.

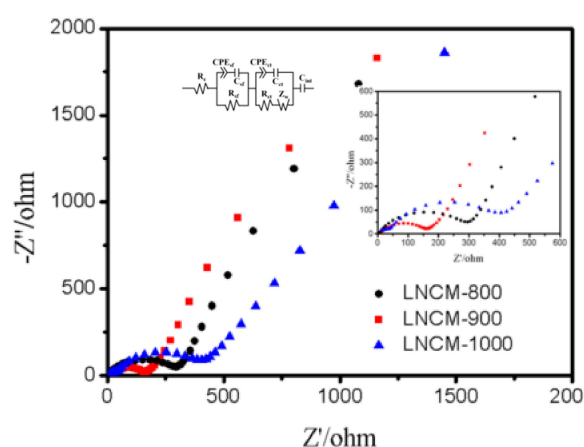
Figure 3b shows the charging and discharging curves of the LNCM-900 at the first, second, and fifth cycles, respectively. As analyzed above, there was a charging platform at 3.9–4.5 V and 4.5 V for the first cycle. The coulombic efficiencies of the electrode were approximately 66.1%, 92.7%, and 91.8% for the first, second, and fifth cycles, respectively. The first-time charge–discharge coulomb

efficiency of LNCM-900 was very low, due to the formation of an SEI film on the surface of the electrode material and an irreversible phase transition process of lithium extraction and oxygen release from  $\text{Li}_2\text{MnO}_3$ . In the second and fifth charge process, the platform around 4.5 V disappeared, the coulombic efficiencies returned to normal, and the corresponding discharge capacities were 242 and 234  $\text{mAh g}^{-1}$ , respectively.

The rate capability of three samples was investigated by cycling at charge/discharge rates range from 0.1C to 5C for 5 cycles and then back to 0.1 C for 5 cycles, as shown in Figure 3c. LNCM-900 exhibited obviously higher discharge capacities than that of LNCM-800 and LNCM-1000. The discharge capacities of LNCM-900 were 252, 188, 164, 136, and 98  $\text{mAh g}^{-1}$  at charge/discharge rates of 0.1, 0.2, 0.5, 1, 2, and 5C, respectively. When the charge/discharge rate was back to 0.1 C after being cycled at 5C, the discharge capacity of LNCM-900 was 216  $\text{mAh g}^{-1}$ , yielding a capacity retention of 86%. The results indicate that the combination of the sucrose-assisted method and a suitable calcination temperature can improve the high-rate capability of the Li-rich layered oxides.

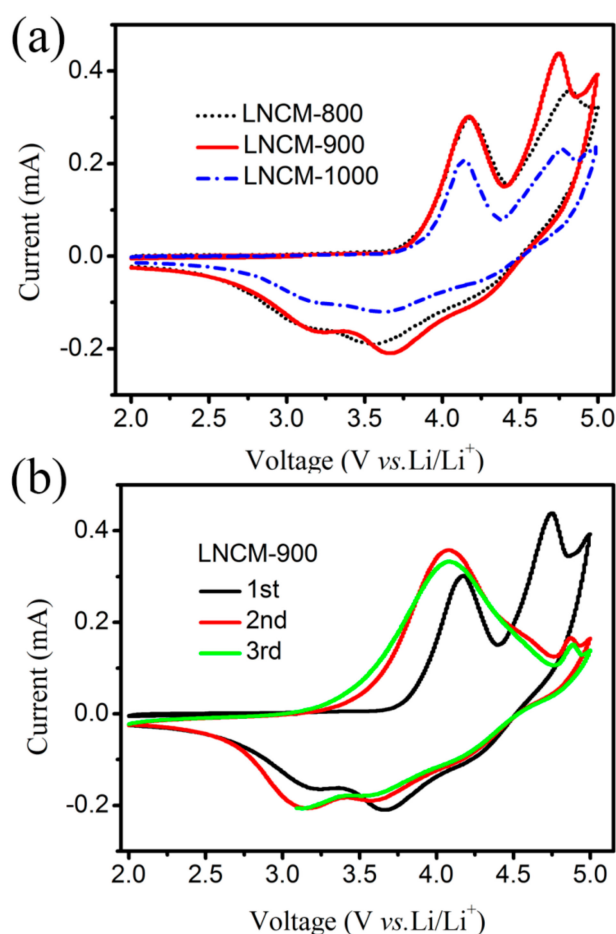
The cycle performance of LNCM-800, LNCM-900, and LNCM-1000 samples was evaluated by repeating the charge/discharge test at 1C, as shown in Figure 3d. After 100 cycles, it was clear that the capacity of LNCM-900 was larger than that of other samples. The first discharge capacity of LNCM-900 was 166  $\text{mAh g}^{-1}$  and maintained 136  $\text{mAh g}^{-1}$  at 1C after 100 cycles, corresponding to a capacity retention of 81%. This result was superior to the cycle performance of samples LNCM-800 and LNCM-1000, indicating the excellent cyclic stability of LNCM-900. The capacity retention of LNCM-1000 was only 45% after 100 cycles. The reasons may be ascribed to the fact that the layered structure of the material is disordered when calcined at a high temperature of 1000 °C and occurs irreversible changes after several cycles, resulting in the discharge capacity decreasing rapidly. The cycle performance of sample LNCM-900 was better than of a hierarchically porous layered lithium-rich oxide  $0.5\text{Li}_2\text{MnO}_3 \cdot 0.5\text{LiMn}_{1/3}\text{Ni}_{1/3}\text{Co}_{1/3}\text{O}_2$  [33].

Figure 4 shows the EIS curves of three samples were composed of a semicircle in the high-frequency region and a sloping line in the low-frequency region, which represents surface charge-transfer resistance ( $R_{ct}$ ) and a semi-infinite warburg diffusion of the lithium-ion in  $\text{Li}[\text{Li}_{0.2}\text{Mn}_{0.56}\text{Ni}_{0.16}\text{Co}_{0.08}]\text{O}_2$ , respectively. Further, EIS plots can be fitted by using an equivalent circuit (inset of Figure 4), which is composed of the solution resistance of the battery ( $R_e$ ), the diffusion resistance of  $\text{Li}^+$  on the material surface ( $R_{sf}$ , also named SEI resistance), charge transfer resistance ( $R_{ct}$ ), Warburg resistance ( $Z_w$ ), the non-ideal capacitance (CPE), and the capacitance of the surface layer ( $C_{sf}$ ) is the charge transfer capacity ( $C_{ct}$ ) and lithium-ion insertion capacitance ( $C_{int}$ ). The  $R_{ct}$  value of LNCM-900 was 160  $\Omega$ , smaller than that of LNCM-800 (298  $\Omega$ ) and LNCM-1000 (406  $\Omega$ ), indicating the fast transport of lithium ions at the electrode/electrolyte interface and improvement of the diffusion ability of lithium ions.



**Figure 4.** The electrochemical impedance spectroscopy (EIS) curves of LNCM-800, LNCM-900, and LNCM-1000.

Cyclic voltammograms (CV) of the as-prepared  $\text{Li}[\text{Li}_{0.2}\text{Mn}_{0.56}\text{Ni}_{0.16}\text{Co}_{0.08}]\text{O}_2$  samples (LCNM-800, LCNM-900, and LNCM-1000) were used to evaluate the redox reaction and the reversibility of the electrochemical process. Figure 5 exhibits the first CV curves of the three samples in the range of 2.0 to 5.0 V at a scan rate of  $0.1 \text{ mV s}^{-1}$ . All samples had two oxidation peaks located at around 4.2 and 4.7 V in the charging process. The peak at around 4.2 V is assigned to the oxidation of metal cations, such as  $\text{Ni}^{2+}$  to  $\text{Ni}^{4+}$  and  $\text{Co}^{3+}$  to  $\text{Co}^{4+}$  [29–33]. Another peak at around 4.7 V corresponds to the extraction of  $\text{Li}^+$  and the irreversible oxygen loss from  $\text{Li}_2\text{MnO}_3$  phase, resulting in the formation of  $\text{Li}_2\text{O}$ , which is consistent of the above analysis in the initial charge and discharge curves. For the discharge curves, an obvious peak (3.6 V) and two weak peaks (3.2 V and 4.3 V, respectively) can be observed. The peaks located at around 3.6 and 4.3 V are associated with the reduction of metal cations, and another peak at around 3.3 V is ascribed to the lithiation of the layered active  $\text{MnO}_2$  [20]. Figure 5b shows CV curves of the LNCM-900 at the first, second, and third cycles, respectively. As analyzed above, after the first cycle, the sharp oxidation peak at around 4.7 V disappears, indicating the removal of the  $\text{Li}_2\text{O}$ .



**Figure 5.** (a) The initial cyclic voltammograms (CV) curves of LCNM-800, LCNM-900, and LNCM-1000, (b) The CV curves of LNCM-900.

#### 4. Conclusions

In conclusion,  $\text{Li}[\text{Li}_{0.2}\text{Mn}_{0.56}\text{Ni}_{0.16}\text{Co}_{0.08}]\text{O}_2$  with high crystallinity and a layered structure was successfully prepared by the sucrose-assisted gel method. The sucrose-assisted method is feasible and effective for fabricating layered lithium-rich materials. The morphology, structure, electrochemical properties were analyzed to explore the best preparation route. XRD showed that the lithium-rich material  $\text{Li}[\text{Li}_{0.2}\text{Mn}_{0.56}\text{Ni}_{0.16}\text{Co}_{0.08}]\text{O}_2$  had a well-organized layered structure. When the  $\text{Li}[\text{Li}_{0.2}\text{Mn}_{0.56}\text{Ni}_{0.16}\text{Co}_{0.08}]\text{O}_2$  sample was obtained by calcining at  $900^\circ\text{C}$ , it exhibits an excellent rate

performance, good cycle stability, and a higher discharge specific capacity ( $252 \text{ mAh g}^{-1}$ ). Its discharge capacity decreased from  $166 \text{ mAh g}^{-1}$  to  $136 \text{ mAh g}^{-1}$  at 1C after 100 cycles, and the capacity retention rate was 81%. The good performance of  $\text{Li}[\text{Li}_{0.2}\text{Mn}_{0.56}\text{Ni}_{0.16}\text{Co}_{0.08}]\text{O}_2$  calcined at  $900^\circ\text{C}$  is due to the fast transport of lithium ions at the electrode/electrolyte interface and improvement of the diffusion ability of lithium ions.

**Author Contributions:** Conceptualization, X.S. and H.H.; synthesis of materials, X.S. and H.H.; electrochemical performances, X.S. and H.H.; analysis of Structure and morphology, X.S. and H.H.; organize the data, X.S., H.H., and W.Z.; writing—original draft preparation, X.S. and H.H.; writing—review and editing, H.H. and W.Z.; funding acquisition, W.Z. All authors have given approval to the final version of the manuscript.

**Funding:** This research was funded by the National Natural Science Foundation, grant number 51801097, and the Industrial Innovation of Applied Fundamental Research, grant number JC2018022, and the Fundamental Research Funds for the Central Universities.

**Conflicts of Interest:** The authors declare no conflict of interest.

## References

1. Armand, M.; Tarascon, J.M. Building better batteries. *Nature* **2008**, *451*, 652–657. [[CrossRef](#)] [[PubMed](#)]
2. Larcher, D.; Tarascon, J.M. Towards greener and more sustainable batteries for electrical energy storage. *Nat. Chem.* **2015**, *7*, 19–29. [[CrossRef](#)] [[PubMed](#)]
3. Dunn, B.; Kamath, H.; Tarascon, J.M. Electrical energy storage for the grid: a battery of choices. *Science* **2011**, *334*, 928–935. [[CrossRef](#)] [[PubMed](#)]
4. Goodenough, J.B.; Park, K.S. The Li-ion rechargeable battery: a perspective. *J. Am. Chem. Soc.* **2013**, *135*, 1167–1176. [[CrossRef](#)] [[PubMed](#)]
5. Thackeray, M.M.; Wolverton, C.; Isaacs, E.D.; Environ, E. Electrical energy storage for transportation—Approaching the limits of, and going beyond, lithium-ion batteries. *Energy Environ. Sci.* **2012**, *5*, 7854–7863. [[CrossRef](#)]
6. Park, J.H.; Cho, J.H.; Lee, E.H.; Kim, J.M.; Lee, S.Y. Thickness-tunable polyimide nanoencapsulating layers and their influence on cell performance/thermal stability of high-voltage  $\text{LiCoO}_2$  cathode materials for lithium-ion batteries. *J. Power Sources* **2013**, *244*, 442–449. [[CrossRef](#)]
7. Wang, G.; Liu, H.; Liu, J.; Qiao, S.; Lu, G.M.; Munroe, P.; Ahn, H. Mesoporous  $\text{LiFePO}_4/\text{C}$  Nanocomposite Cathode Materials for High Power Lithium Ion Batteries with Superior Performance. *Adv. Mater.* **2010**, *22*, 4944–4948. [[CrossRef](#)]
8. Lee, M.-J.; Lee, S.; Oh, P.; Kim, Y.; Cho, J. High Performance  $\text{LiMn}_2\text{O}_4$  Cathode Materials Grown with Epitaxial Layered Nanostructure for Li-Ion Batteries. *Nano Lett.* **2014**, *14*, 993–999. [[CrossRef](#)]
9. Yoshio, M.; Wang, H.; Fukuda, K.; Umeno, T.; Abe, T.; Ogumi, Z. Improvement of natural graphite as a lithium-ion battery anode material, from raw flake to carbon-coated sphere. *J. Mater. Chem.* **2004**, *14*, 1754–1758. [[CrossRef](#)]
10. Han, Z.J.; Yabuuchi, N.; Shimomura, K.; Murase, M.; Yui, H.; Komaba, S. High-capacity Si-graphite composite electrodes with a self-formed porous structure by a partially neutralized polyacrylate for Li-ion batteries. *Energy Environ. Sci.* **2012**, *5*, 9014–9020. [[CrossRef](#)]
11. Xiang, H.F.; Zhang, X.; Jin, Q.Y.; Zhang, C.P.; Chen, C.H.; Ge, X.W. Effect of capacity matchup in the  $\text{LiNi}_{0.5}\text{Mn}_{1.5}\text{O}_4/\text{Li}_4\text{Ti}_5\text{O}_{12}$  cells. *J. Power Sources* **2018**, *183*, 355–360. [[CrossRef](#)]
12. Ellis, B.L.; Lee, K.T.; Nazar, F.L. Positive Electrode Materials for Li-Ion and Li-Batteries. *Chem. Mater.* **2010**, *22*, 691–714. [[CrossRef](#)]
13. Zhu, Y.; You, J.; Huang, H.; Li, G.; Zhou, W.; Guo, J. Facile synthesis and electrochemical properties of layered  $\text{Li}[\text{Ni}_{1/3}\text{Mn}_{1/3}\text{Co}_{1/3}]\text{O}_2$  as cathode materials for lithium-ion batteries. *Front. Mater. Sci.* **2017**, *11*, 155–161. [[CrossRef](#)]
14. Xie, Y.; Saubanere, M.; Doublet, M.L. Requirements for reversible extra-capacity in Li-rich layered oxides for Li-ion batteries. *Energy Env. Sci.* **2017**, *10*, 266–274. [[CrossRef](#)]
15. Hy, S.; Liu, H.; Zhang, M.; Qian, D.; Hwang, B.J.; Meng, Y.S. Performance and design considerations for lithium excess layered oxide positive electrode materials for lithium ion batteries. *Energy Environ. Sci.* **2016**, *9*, 1931–1954. [[CrossRef](#)]

16. Jarvis, K.A.; Deng, Z.; Allard, L.F.; Manthiram, A.; Ferreira, P.J. Atomic Structure of a Lithium-Rich Layered Oxide Material for Lithium-Ion Batteries: Evidence of a Solid Solution. *Chem. Mater.* **2011**, *23*, 3614–3621. [[CrossRef](#)]
17. Rozier, P.; Tarascon, J.M. Review—Li-Rich Layered Oxide Cathodes for Next-Generation Li-Ion Batteries: Chances and Challenges. *J. Electrochem. Soc.* **2015**, *162*, A2490–A2499. [[CrossRef](#)]
18. Kobayashi, G.; Irii, Y.; Matsumoto, F.; Ito, A.; Ohsawa, Y.; Yamamoto, S.; Cui, Y.; Son, J.Y.; Sato, Y. Improving cycling performance of Li-rich layered cathode materials through combination of Al<sub>2</sub>O<sub>3</sub> -based surface modification and stepwise precycling. *J. Power Sources* **2016**, *303*, 250–256. [[CrossRef](#)]
19. Zhao, T.; Li, L.; Chen, R.; Wu, H.; Zhang, X.; Chen, S.; Xie, M.; Wu, F.; Lu, J.; Amine, K. Design of surface protective layer of LiF/FeF<sub>3</sub> nanoparticles in Li-rich cathode for high-capacity Li-ion batteries. *Nano Energy* **2015**, *15*, 164–176. [[CrossRef](#)]
20. Chen, D.; Tu, W.; Chen, M.; Hong, P.; Zhong, X.; Zhu, Y.; Yu, Q.; Li, W. Synthesis and performances of Li-Rich@AlF<sub>3</sub>@Graphene as cathode of lithium ion battery. *Electrochim. Acta* **2016**, *193*, 45–53. [[CrossRef](#)]
21. Chen, D.; Yu, Q.; Xiang, X.; Chen, M.; Chen, Z.; Song, S.; Xiong, L.; Liao, Y.; Xing, L.; Li, W. Porous layered lithium-rich oxide nanorods: Synthesis and performances as cathode of lithium ion battery. *Electrochim. Acta* **2015**, *154*, 83–93. [[CrossRef](#)]
22. Penki, T.R.; Shanmugasundaram, D.; Munichandraiah, N. Porous lithium rich Li<sub>1.2</sub>Mn<sub>0.54</sub>Ni<sub>0.22</sub>Fe<sub>0.04</sub>O<sub>2</sub> prepared by microemulsion route as a high capacity and high rate capability positive electrode material. *Electrochim. Acta* **2014**, *143*, 152–160. [[CrossRef](#)]
23. Qian, Y.; Deng, Y.; Shi, Z.; Zhou, Y.; Zhuang, Q.; Chen, G. Sub-micrometer-sized LiMn<sub>1.5</sub>Ni<sub>0.5</sub>O<sub>4</sub> spheres as high rate cathode materials for long-life lithium ion batteries. *Electrochem. Commun.* **2018**, *27*, 92–95. [[CrossRef](#)]
24. Xu, B.; Fell, C.R.; Chi, M.; Meng, Y.S. Identifying surface structural changes in layered Li-excess nickel manganese oxides in high voltage lithium ion batteries: A joint experimental and theoretical study. *Energy Environ. Sci.* **2011**, *4*, 2223–2233. [[CrossRef](#)]
25. Xiang, X.; Li, W. Significant influence of insufficient lithium on electrochemical performance of lithium-rich layered oxide cathodes for lithium ion batteries. *Electrochim. Acta* **2014**, *133*, 422–427. [[CrossRef](#)]
26. Shi, S.J.; Tu, J.P.; Tang, Y.Y.; Yu, Y.X.; Zhang, Y.Q.; Wang, X.L.; Gu, C.D. Combustion synthesis and electrochemical performance of Li[Li<sub>0.2</sub>Mn<sub>0.54</sub>Ni<sub>0.13</sub>Co<sub>0.13</sub>]O<sub>2</sub> with improved rate capability. *J. Power Sources* **2013**, *228*, 14–23. [[CrossRef](#)]
27. Ohzuku, T. Electrochemistry and Structural Chemistry of LiNiO<sub>2</sub> (R3m) for 4 Volt Secondary Lithium Cells. *J. Electrochem. Soc.* **1993**, *140*, 1862–1870. [[CrossRef](#)]
28. Zhu, Z.; Zhu, L. Synthesis of layered cathode material 0.5Li<sub>2</sub>MnO<sub>3</sub>·0.5LiMn<sub>1/3</sub>Ni<sub>1/3</sub>Co<sub>1/3</sub>O<sub>2</sub> by an improved co-precipitation method for lithium-ion battery. *J. Power Source* **2014**, *256*, 178–182. [[CrossRef](#)]
29. Qiao, Q.Q.; Li, G.R.; Wang, Y.L.; Gao, X.P. To enhance the capacity of Li-rich layered oxides by surface modification with metal–organic frameworks (MOFs) as cathodes for advanced lithium-ion batteries. *J. Mater. Chem. A* **2016**, *4*, 4440–4447. [[CrossRef](#)]
30. Xia, Q.; Zhao, X.; Xu, M.; Ding, Z.; Liu, J.; Chen, L.; Ivey, D.; Wei, W. A Li-rich Layered@Spinel@Carbon heterostructured cathode material for high capacity and high rate lithium-ion batteries fabricated via an in situ synchronous carbonization-reduction method. *J. Mater. Chem. A* **2015**, *3*, 3995–4003. [[CrossRef](#)]
31. Martha, S.K.; Nanda, J.; Veith, G.M.; Dudney, N.J. Electrochemical and rate performance study of high-voltage lithium-rich composition: Li<sub>1.2</sub>M<sub>0.525</sub>Ni<sub>0.175</sub>Co<sub>0.1</sub>O<sub>2</sub>. *J. Power Sources* **2012**, *199*, 220–226. [[CrossRef](#)]
32. Hy, S.; Felix, F.; Rick, J.; Su, W.-N.; Hwang, B.J. Direct In situ Observation of Li<sub>2</sub>O Evolution on Li-Rich High-Capacity Cathode Material, Li [Ni<sub>x</sub>Li<sub>(1-2x)/3</sub>Mn<sub>(2-x)/3</sub>] O<sub>2</sub> (0 ≤ x ≤ 0.5). *J. Am. Chem. Soc.* **2014**, *136*, 999–1007. [[CrossRef](#)] [[PubMed](#)]
33. Chen, M.; Xiang, X.; Chen, D.; Liao, Y.; Huang, Q.; Li, W. Polyethylene glycol-assisted synthesis of hierarchically porous layered lithium-rich oxide as cathode of lithium ion battery. *J. Power Sources* **2015**, *279*, 197–204. [[CrossRef](#)]

